# MicroElectroMechanical Systems (MEMS) for applications in acoustics

Rui Sampaio
rui.sampaio@ist.utl.pt

Instituto Superior Técnico, Lisboa, Portugal

December 2013

**Abstract**

The success of MicroElectroMechanical systems (MEMS) as small microphones for mobile application verified in recent years is expected to be reflected in MEMS loudspeakers. Some advantages include very low power consumption, low fabrication cost and integrability with CMOS technology.

The aim of this work was to present a new fabrication process based on PECVD amorphous silicon for ultra-low power electrostatic MEM loudspeakers together with a consistent theoretical description and initial experimental characterization. The first approach was carried by extending the well-developed process for thin bridges and cantilevers at INESC-MN. Because of the incompatibility of this process with a loudspeaker application a second generation process was developed. The simplicity of the process is lost but important aspects such as low temperature, CMOS compatibility and the use of typical materials in MEMS processing are retained.

A working prototype for the second generation is presented and the first generation process is revisited for a first study on the mechanical properties of the structures. Resonance frequency measurements in a pressure controlled environment are provided together with absolute deflection measurements in the audible-rage. Finally a general discussion is provided setting design rules for further development.

**Keywords:** MEMS, Electrostatic, Loudspeaker, Amorphous Silicon

## 1. Introduction

MEMS microphones are currently being adopted for many portable devices such as smartphones, tablets or laptops with a projected revenue of $493.5 million for 2012 and $667.0 million by 2015 (IHS iSuppli Research, January 2012) and are replacing the conventional electret condenser microphones (ECM) [1]. Advantages of MEMS microphones include immunity to electromagnetic interference and radio frequency radiation (for digital microphones), directionality, noise cancellation by using arrays of microphones, on-chip integration, CMOS compatibility and better performance and stability metrics [5].

The microphone working principle is the transduction of acoustical energy into electrical energy by conversion of mechanical movement to an electrical signal. Transduction mechanisms for silicon MEMS include piezoelectric, piezoresistive and condenser [19]. In piezoelectric transduction the deflection of the sensing diaphragm is converted into voltage drop, sensed by a top and bottom electrode on the diaphragm. Piezoresistive transduction is based on the change of resistance due to the induced strain on the diaphragm. Sensing is usually accomplished in a Wheatstone bridge. Condenser transduction is based on the change of capacitance between the diaphragm and a sensing gate. This is most widely and most successful implementation of MEMS microphones nowadays.

MEMS loudspeakers are expected to share the success of their microphones counterpart. Market competitive product are however more difficult to come by due to the need of large deflection or large areas of actuation. Possible applications include mobile devices ([4], [9], [10], [14], [3]), hearing aids ([7], [8]) and ultrasonic systems ([16], [11]) using different mechanisms of actuation such as piezoelectric, electrostatic, electrodynamic and thermoacoustic.

Piezoelectric actuation is based on the contraction of a piezoelectric block in between two electrodes by applying an external electric field. Typical materials include ZnO and PZT usually deposited on top of a silicon nitride layer for mechanical control and stability. Piezoelectric loudspeakers enjoy of a robust fabrication process and are easily scalable for large areas, as far as hundreds of $mm^2$.

Also they radiate as a monopole, circumventing the need for front-side / back-side isolation. Their disadvantage is the presence of a polarization - electric field (PE) hysteresis curve and a low first resonance frequency leading to a very non-linear response in the audible range ([13], [12], [22], [10]). Electrodynamic actuation is based on the Lorentz force. In the presence of a magnetic field a current line experiences a force perpendicular to the current line and the magnetic field. The magnetic field is typically generated by a permanent magnet. Metal tracks are incorporated in the membrane and the deflection is controlled by the current's magnitude. Soft magnets are usually present to focus the permanent magnetic field. The electrodynamic transduction mechanism is the most common in the literature with several different proposed devices ([21], [17], [3], [8], [2], [20]). Electrostatic actuation uses the reverse principle of capacitive microphones. The membrane is driven by the electrostatic force imposed by an external source. The fixed electrode is called the *gate electrode* while the suspended electrode is called the membrane or diaphragm. Electrostatic actuation is well suited very-low power application and integrability with CMOS dies. The main disadvantages of electrostatic driving is a high voltage cost and low deflection amplitudes ([16], [9], [18]).

Electrostatic MEMS loudspeakers present some advantages over electrodynamic or piezoelectric driven loudspeakers — they can be integrated in a CMOS dies, using common materials such as silicon, aluminium or silicon dioxide, they have no DC power consumption and require very low alternating current amplitude avoiding local heating and material deterioration. Unfortunately they present strong disadvantages such as high driving voltages and low amplitudes of deflection when compared to electrodynamic actuation, for example. The devices proposed here aim for a very low driving voltage of 3.3 V, with deflection of the order of 1 $\mu m$. The design and choice of materials itself also allows arraying of single structures, thus proving lower acoustic waveform deformation over large areas of actuation and better control over the membranes mechanical properties. For the particular application of hearing aids, low driving voltages with ultra-low power consumption and large areas of actuation are required. The purposed devices deliver on all these requirements. Moreover, the novelty of the fabrication process in this field, overcoming the large voltage cost drawback, allows the possibility of entering on the virtually unexplored market of MEMS loudspekers for hearing aids. Finally, large area MEMS have strong applications in other areas such as microfluidics, physical sensors, biosensors or electronic components. While the process development and structural characterization and optimization is acoustic oriented, valuable know-how is to be retained for such other applications.

## 2. Fabrication

Two fabrication processes were explored — a first generation process resulting from the extension of a previously well developed process for thin beams and bulk resonators and a second generation process developed in view of the incompatibility of the former for a loudspeaker application.

### 2.1. First generation

The first approach to the problem was to extended the well developed standard process for thin beams and bulk resonators at *INECS-MN* to thin plates with large areas, held by four tethers (Figure 1). The process is summarized in Figure 2.1 —(a) The process starts with the cleaning of a two by one inch glass substrate; (b) A sputtered TiW layer is patterned by RIE to define the gate electrode; (c) Sputtered aluminium is used to defined the sacrificial layer by wet etching; (d) the structural double layer a-Si:H/TiW is patterned by a single step of RIE and (e, f) the substrate is diced into individual dies and the sacrificial layer is removed by wet etching, releasing the structure.

### 2.2. Second generation

The proposed structures for the second generation of loudspeakers are depicted in Figure 4 — a clamped a-Si:H plate (a) and a suspended square plate (b) held by four tethers. Each membrane is separated by an *air gap* from a gate electrode for electrostatic actuation and the lateral dimensions, membrane side or diameter, are much larger than the air gap height or the thickness of the membrane.

The gate electrode and substrate are perforated from side to side to introduce vent holes in order to decrease the compression of air between the membrane and substrate and allow the back-wave to propagate. Also, to assure a constant spatial distribution of the electrical potential through out the membrane, a metal layer is present on top of the membrane, with thickness much smaller than the membrane's. Finally, aluminium oxide ($Al_2O_3$) layers are introduce between the gate and substrate and between the gate and membrane in the case of the clamped geometries for electrical isolation.

The proposed process is a 7 layer process with one layer on the back-side of the sample plus 6 layers on the front-side of the sample. A summary of the process is depicted in figure 3

Alignment marks are first etched on both sides of a double side polished, undoped $< 100 >$ silicon wafer and individual rectangular substrates with 2 inch by 1 inch are then diced from the silicon wafer. Sputtered alumina ($Al_2O_3$) is first patterned with a

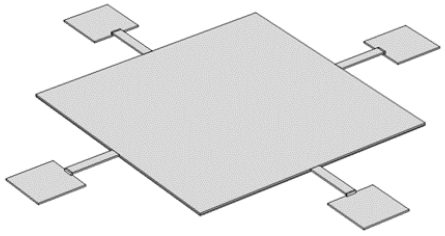

(a)

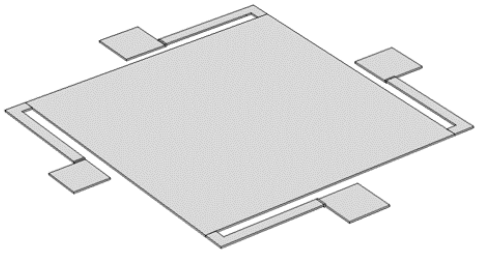

(b)

Figure 1: 3D models of the first generation loudspeakers for the (a) *perpendicular* geometry and (b) *parallel* geometry.

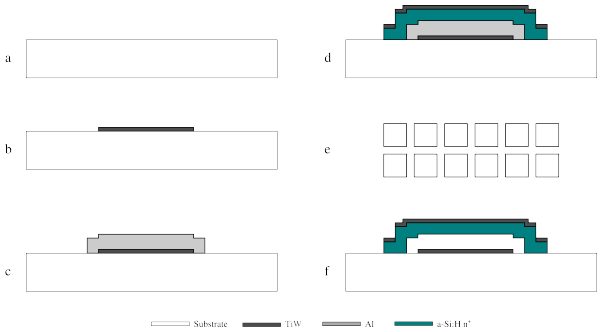


Figure 2: Process overview of the first generation loudspeakers. a) 2 inch by 1 inch glass substrate; b)Patterning of the TiW gate; c) Patterning of the Al sacrificial layer; d) Patterning of the a-Si:H/TiW structural layer; e) Dicing and f) structure release. Not to scale.

wet etch on the back-side of the sample. This will be used latter on as the hard mask for the DRIE of the substrate. A similar alumina layer is then patterned on the front-side of the sample for electrical isolation of the substrate. The gate contacts are then defined using sputtered aluminium together with a wet etch. A silica layer is introduce for passivation of the underling Al layer. Another alumina layer is patterned on top of the gate layer for electrical isolation between the gate and membrane. The $SiO_2$ sacrificial layer is then defined using a PECVD step together with a RIE step. The a-Si:H/Al structural layer is deposited using a PECVD step for the a-Si:H and a sputter deposition for the aluminium. The aluminium is first patterned using a wet etch and the a-Si:H using a RIE step. The substrate is then perforated from the back-side using a DRIE step. The sample is diced into individual dies for the release step with HF vapor finishing the microfabrication process. . For the suspended square geometry the process is almost exactly the same with the difference that the alumina layer for electrical isolation between gate and membrane and the $SiO_2$ passivation layer are not present.

Due to the complexity of the process and the requirement for optimization on several steps, a simpler process was used for optimization of the deposition of a-Si:H film and provide an initial experimental characterization. The process is here referred as the *amorphous silicon deposition test process*. It replicates every step of the full process with the exception of the DRIE step (and the back-side alumina hard mask). Small perforation are introduced on the membrane instead to allow the etchant to reach the sacrificial layer.

## 3. Theoretical Description

The general form of the response of a thin plate to an harmonic excitation can be written as the sum of all natural modes for the particular geometry, namely,

$$w(\eta,\xi,\tau) = \sum_{n=1}^{\infty} \frac{G_n}{(\Omega_n^4 - \Omega^4) + j2\zeta\Omega^2} W_n(\eta,\xi) e^{j\Omega^2\tau} \tag{1}$$

where $w(\eta,\xi,\tau)$ is the complex normalized displacement of the membrane at the normalized points $\eta = x/a$ and $\xi = y/a$ at the normalized time $\tau = t/t_p$, $a$ is the side or radius of the plate, $t_p = \rho t a^4/D$, $\rho$ is the density of the material, $t$ is the thickness of the plate, $D = Et^3/12(1-\nu^2)$ is the rigidity of the plate, $E$ is the Young's modulus, $\nu$ is the Poisson coefficient, $\Omega_n$ is the n'th natural frequency, $W_n$ is the n'th natural mode, $G_n = (1/N_n)\int dA F_a(\eta,\xi) W_n$ is a weighting factor determining the extent of the excitation of the n'th mode, $N_n = \int dA W_n^2$ is a normalization factor, $F_a(\eta,\xi)$ is the applied load, $\zeta = ca^4/D$ is the damping parameter, $c$ is the damp-

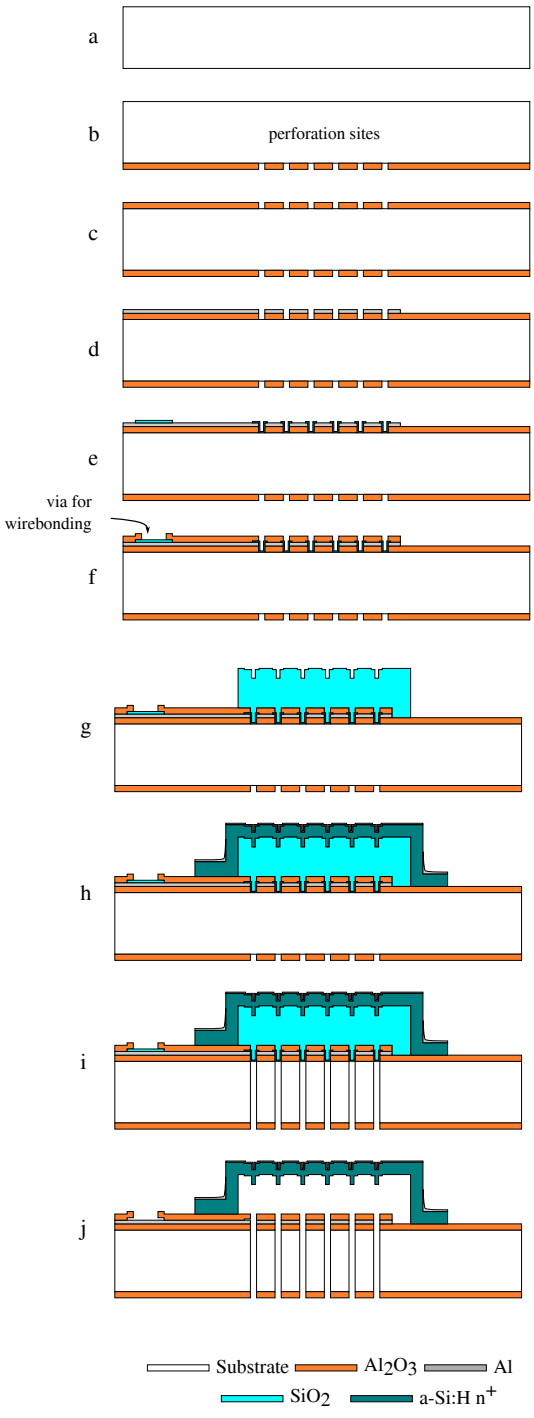


Figure 3: Second generation loudspeaker process summary. Image not to scale.

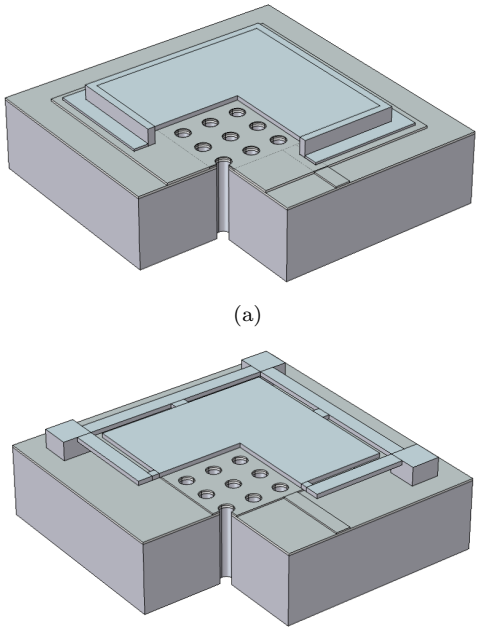

(a)

(b)

Figure 4: 3D models of the rectangular clamped geometry and the suspended-square geometry. Not to scale.

ing coefficient and $\Omega = \sqrt{2\pi f t_p}$ is the normalized driving frequency. For thin beams, the deflection only depends on one direction, say $x$, and $D$ should be replaced by $EI$ where $I = wt^3/12$ for rectangular cross-section, $w$ is the width of the beam.

Depending on the case to be analysed, clamped rectangular plates, clamped circular plates or suspended squares, the coefficient $G_n$ and the normal models $W_n$ will take on different form accordingly to the specific case. Figure 5 shows the frequency spectrum for a thin-beam, a clamped rectangular plate and a circular rectangular plate for the case of no axial stress. It is noted that the frequency spectrum of the thin-beam does not correspond to the frequency spectrum of the suspended square geometry but it provides important information since the stiffness of the system is essentially determined by the tethers.

### 3.1. One degree of freedom approximation

For frequencies bellow the first resonance and around it the system can be approximated by a driven liner damped spring-mass system using equivalent lumped parameters — an effective mass ($m_0$), an elastic constant ($k_0$) and a damping coefficient ($c_d$). Assuming that the driving force can be separated into a static component $F_0$ and an harmonic component $F^\omega \cos(\omega t)$, and the displacement is much smaller the air gap, the equilibrium solution

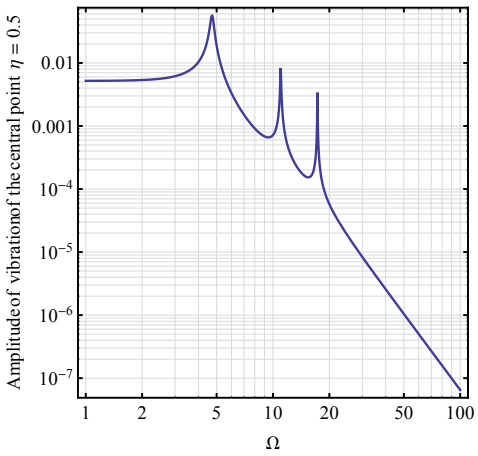


(a)

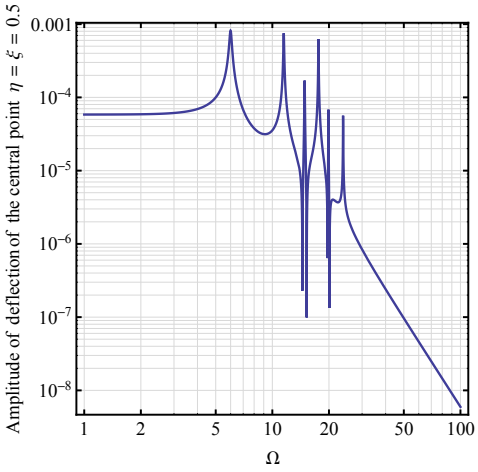


(b)

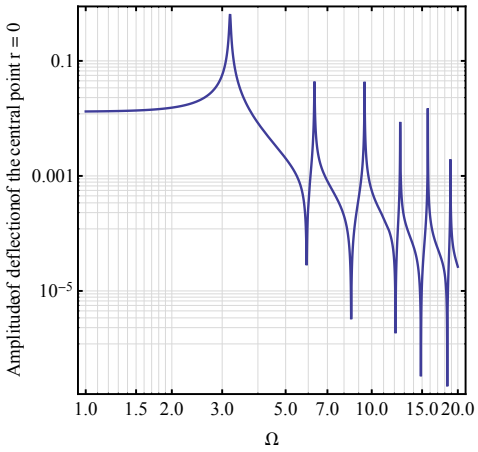


(c)

Figure 5: Normalized frequency spectrum for (a) a thin-beam, (b) a clamped rectangular plates and (c) a clamped circular plate.

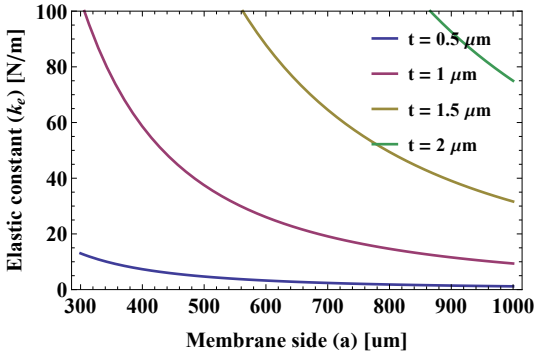


(a)

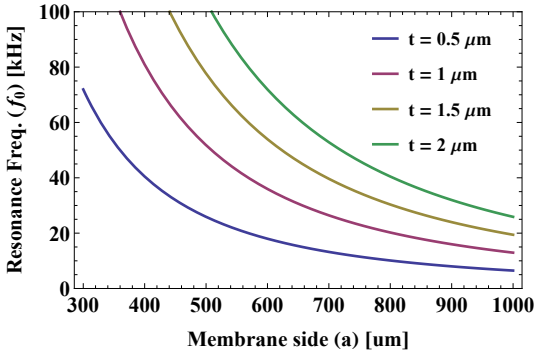


(b)

Figure 6: Elastic constant (a) and resonance frequency (b) as a function of the side and thickness of a rectangular membrane without axial stress. The case for circular plates yields very similar values as can be seen from table (1).

can be written as

$$x(t) = x_0 + \frac{F^{\omega}/m_0}{\sqrt{(\omega_0^2 - \omega^2)^2 - c_d^2\omega^2/m_0^2}} \cos(\omega t + \phi) \tag{2}$$

where $x_0$ is the equilibrium static displacement caused by $F_0$, $\phi$ is the phase shift relative to the excitation force and $\omega_0$ is the angular resonance frequency. The elastic constant is taken considering the maximum displacement for a static uniform load, the resonance frequency must match the first resonance frequency of the thin plate and the effective mass is given by the well known relation $m_0 = k_0/w_0^2$. These parameters are summarized in Table 1 for the three geometries presented here. Figure 6 illustrates the range of values expected for the resonance frequency and elastic constant for the case of rectangular membranes with axial stress and Figure 7 shows the effect of the axial stress on the first resonance frequency of circular membranes highlighting the pronounced effect of this parameter.

| | Resonance frequency ($f_0$) | Elastic constant ($k_0$) | Effective mass ($m_0$) |
|---|---|---|---|
| Square membrane | $5.72797\sqrt{\frac{D}{\rho t a^4}}$ | $787.402\frac{D}{a^2}$ | $0.607904\ \rho t a^2$ |
| Circular membrane | $1.6259\sqrt{\frac{D}{\rho t R^4}}$ | $64\pi\frac{D}{R^2}$ | $0.613243\ \rho t \pi R^2$ |
| Suspended square | $4.411\sqrt{\frac{EI}{L_b^3 \rho t(1.5344 w L_b + a^2)}}$ | $\frac{768EI}{L^3}$ | $\rho t(1.5344 w L_b + a^2)$ |

Table 1: First resonance frequency, elastic constant and effective mass for the square and circular membranes and for the suspended square without axial stress. For circular membranes, $R$ is the radius of the membrane.

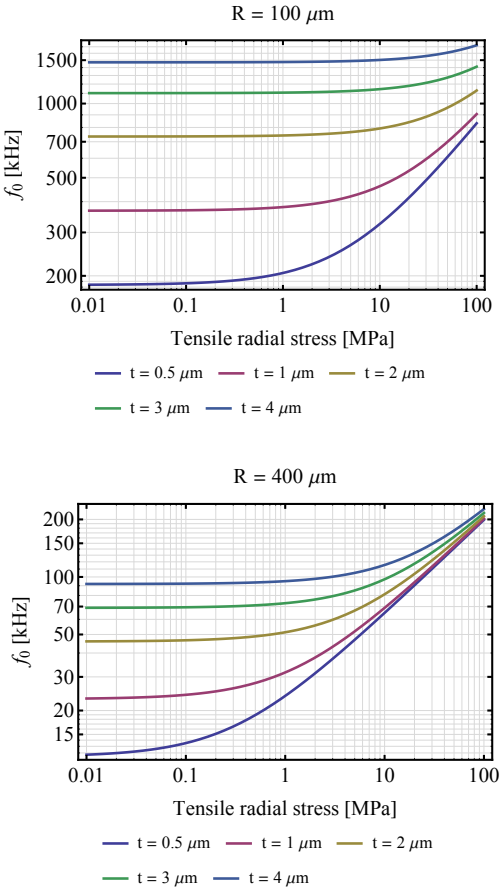


Figure 7: Effect of radial tensile stress on the first resonance frequency of circular membranes with 100 $\mu m$ radius (top) and 400 $\mu m$ radius (bottom).

## 4. Experimental characterization

Two distinct experimental setups were used — one for high frequency characterization at low pressure and one for quasi-DC and audible range measurements. The former highlights intrinsic mechanical properties of the resonators such as resonance frequencies and axial stress while the later allows for measurements of absolute deflection in the audible range at room pressure and temperature.

### 4.1. Quasic-DC and audible range setup

This simple setup comprises an laser, focused on the membrane, and a quadrant photodiode detector aligned with the reflected beam off the membrane. The current generated from the detector is converted to a potential difference by a transimpedance amplifier and fed to a lock-in amplifier, synchronized with the signal generator that is exciting the membrane. The displacement of the beam is proportional to the displacement of the membrane with

$$\delta = \sqrt{2}/2\ \zeta V_{AB} = \zeta {V_{AB}}^{\text{out}} \tag{3}$$

where $\delta$ is the amplitude of vibration of the plate, $V_{AB}^{\text{out}}$ is the value read by the lock-in and $\zeta$ is the proportionality constant to be determined experimentally for each measurement session.

First generation structures alone were characterized using the quasi-DC setup. The structures are $\sim 2\ \mu m$ thick with a target air gap of $1.5\ \mu m$. All the results presented are for the perpendicular geometry with $20\ \mu m$ wide tethers.

Figure 8 (a) shows the frequency spectrum of a $300\ \mu m$ by $300\ \mu m$ membrane held by $200\ \mu m$ long tethers in the audible range.

Figure 8 (b) shows the response of a $500\ \mu m$ by $500\ \mu m$ membrane held by $100\ \mu m$ long tethers at constant frequency (20 Hz) and DC bias (10 V) as a function of the amplitude of the input sinusoidal signal.

Further characterization on these structures was not carried because of their incompatibility with a loudspeaker application (see bellow).

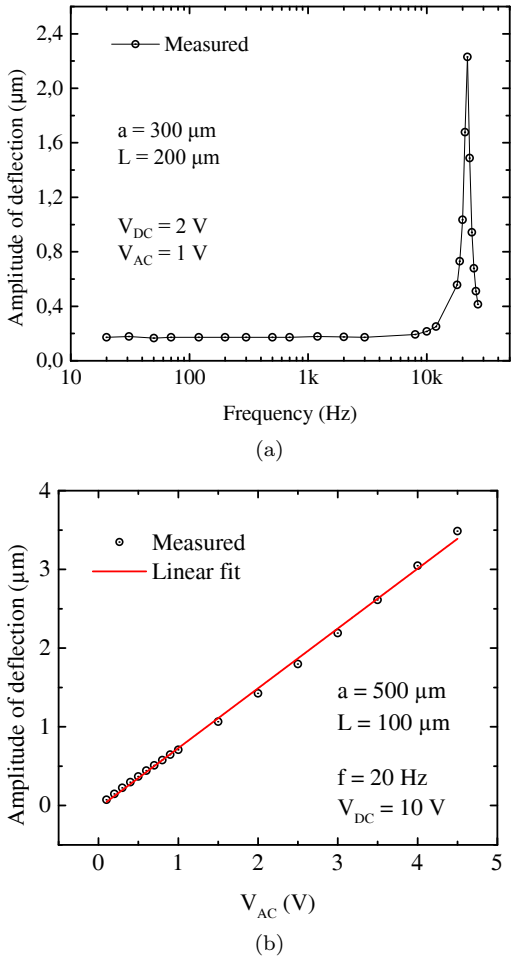


Figure 8: (a) Frequency spectrum in the audible range of a 300 $\mu m$ by 300 $\mu m$ membrane held by 200 $\mu m$ long tethers and (b) amplitude of deflection at 20 Hz of a 500 $\mu m$ by 500 $\mu m$ membrane held by 100 $\mu m$ long tethers at constant DC bias as a function of the input excitation signal.

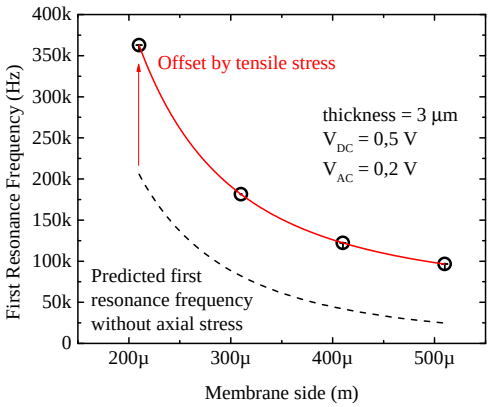


Figure 10: First resonance frequency as a function of the side of the membrane for the suspended square geometry with in-plane tensile stress.

4.2. High frequency detection setup

The high frequency detection setup also uses an optical detection method but instead of a quadrant detector it uses a APD detector (*Hamamatsu C5331*) connected to a network analyzer (HP Network Analyser 4195A). Because the detector has a low frequency cut around 4 kHz this setup is only used for measurement above 50-100 kHz and no information about absolute deflection is provided. Instead, higher modes of vibration can be detected in a pressure controlled chamber with information about mode shape a quality factor. An external source is used to set a DC bias and a the membrane is excited harmonically by the network analyser. The output of the detector is fed to the network analyser. The sample is wire bonded to a chip carrier and placed on a pressure controlled chamber. The setup is described in detail elsewhere [6].

Suspended square membranes were characterized for the first generation process. Membranes 3 $\mu m$ thick with an air gap height of 1 $\mu m$ and sides from 210 $\mu m$ up to 710 $\mu m$ were fabricated. The frequency spectrum from 100 kHz to 2 MHz was measured and plotted in Figure 9 for the 210, 410, 610 and 710 membranes.

Figure 10 shows the dependence of the first resonance mode with the dimensions of the tethers side highlighting the offset of the tensile stress on the resonance frequency.

Clamped membranes were fabricated using the a modified version of the glass-aluminium process and using the silicon-silica process for the amorphous silicon deposition tests. Figure 11 shows the frequency spectrum of a clamped rectangular membrane with 500 $\mu m$ radius for the glass-aluminium process. The first resonance mode predicted for these structures is around 155 kHz which suggests an in-plane stress value between 10 MPa to 100 MPa. This is in line with the values expected for

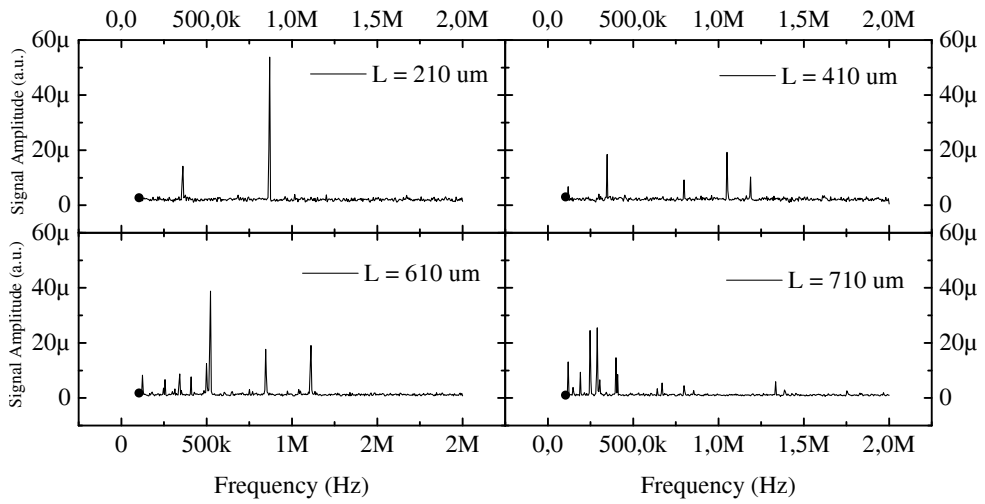


Figure 9: Frequency spectrum overview for the suspended square for different membrane dimensions.

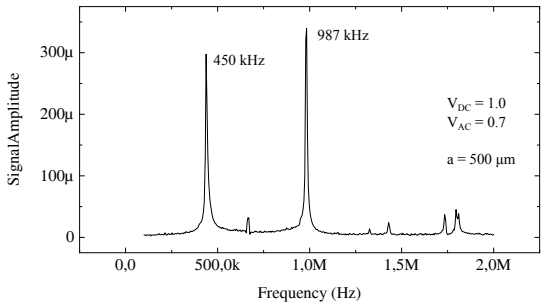


Figure 11: Frequency spectrum of a clamped rectangular membrane with 500 $\mu m$ radius using the modified aluminium-glass process.

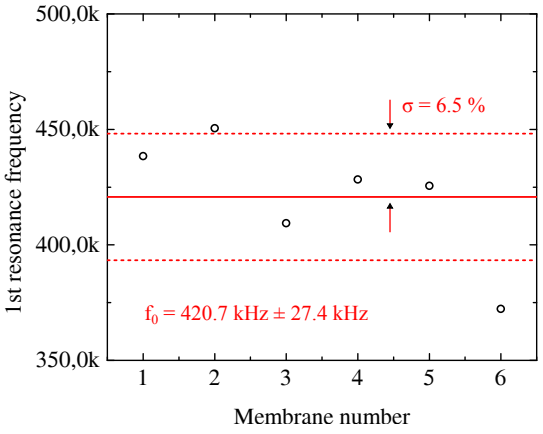


Figure 12: First resonance frequency variation across a single die of 500 $\mu m$ clamped membranes showing a standard deviation of 6.5 %.

this fabrication process.

Figure 12 shows the variation of the first resonance for the equal membranes across the die indicating good reproducibility. The mean calculated resonance frequency is 420.7 kHz with a standard deviation of 27.4 Hz corresponding to 6.5 % of the mean value. This is an important assessment if arraying is required to assure that all membranes show minimal variation in their mechanic characteristics.

Finally, Figure 13 shows a SEM micrograph of a 800 $\mu m$ side clamped membrane using the silicon-silica process for the amorphous silicon deposition tests and Figure 14 shows the corresponding frequency spectrum The membranes are 3 $\mu m$ thick. Although these first structures shows some cracks over the border, which probably is the origin of the high number of resonances, and there is still some problems during the structure release to be overcome the realization of the first standing and vibrating membranes for the newly developed process is definitely a landmark.

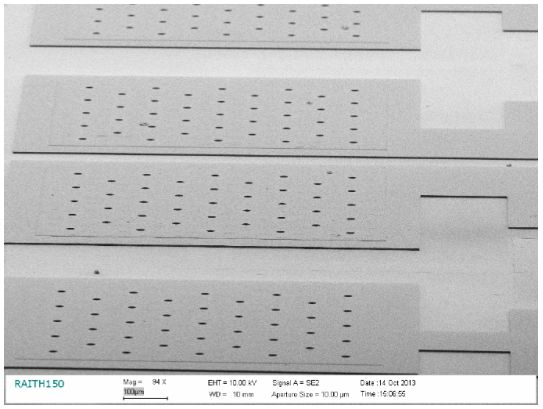


Figure 13: Second generation released 800 $\mu$ clamped membranes fabricated using the amorphous silicon deposition test process.

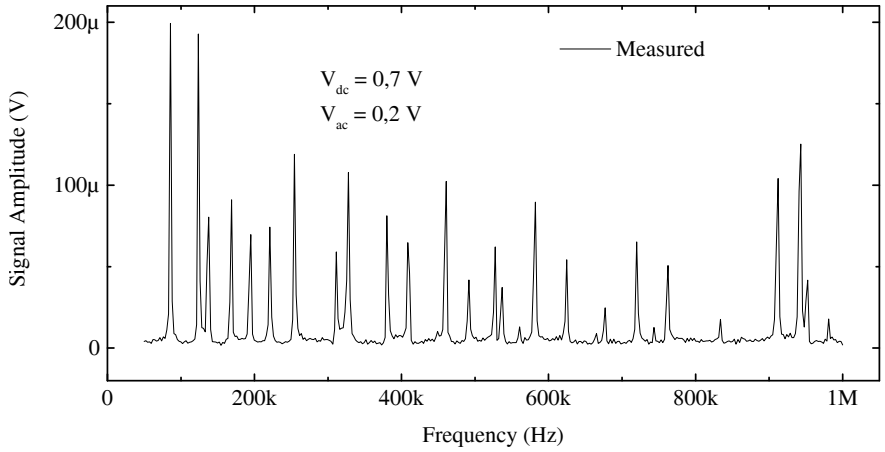


Figure 14: Frequency spectrum of a 800 $\mu m$ clamped membrane for the silicon-silica process.

## 5. Discussion and Conclusion

The first generation structures were design as an extension of a well developed microfabrication process for amorphous silicon thin beams and plates. This is an attractive process due to its low temperature characteristics, great flexibility on the choice of substrate and overall simplicity. Unfortunately this geometry proved to be inconsistent for the realization of a loudspeaker. A suspended membrane radiates like a dipole (see for example [15]) meaning that the pressure immediately above a bellow the membrane are equal and opposite or, in other words, the front-wave and back-wave are in complete opposition of phase.The second generation structures were design considering the limitation of the first generation ones. The perforation of the substrate proved to be indispensable based on several numerical simulations (results not shown). Due to technology limitations the substrate had to be change to crystalline silicon to allow back-side/front-side alignment, material compatibility and the etch of the perforations. The necessity for complete physical isolation of the back-side and front-side volumes is not clear and for this reason both clamped structure and open structures are presented. Open structures have particular advantages over clamped ones such as simplification in the fabrication process, more tolerance to the intrinsic stress of the structural layer and more degrees-of-freedom for performance optimization.

There are several degree-of-freedom such as area, thickness, bias voltage or perforation density that can affect the overall behaviour of the system, each one of which playing a particular role. Through both theoretical and experimental data several conclusions are drawn setting guidelines for further investigation on the topic. It is clear that single structures with side or diameter of the order of millimetres are not straightforwardly realizable without fine optimization of the intrinsic stress of the a-Si:H structural layer. The same is valid for the thickness of such layer, where a narrow margin between 1 to 3 $\mu m$ exists imposed by the technology. Extensive experimental data must be collected for different geometries in order to provide faithful information on non-linear parameters such as squeeze-film damping or electrostatic force in a large-deflection regime, together with the limitation imposed by the technology available.

### 5.1. Achievements

The microfabrication process for an amorphous silicon electrostatic actuated loudspeaker for ultra low power consumption applications was presented. The proposed process allows different geometries compatible with a loudspeaker application and also introduce new concepts not yet present in the market or literature. Moreover typical materials in MEMS processing are used facilitating the transition to a possible production scale. The minimal dependence on the substrate also shows great promising for new trends such as processing on glass and flexible substrates.

Parallel to the process development a consistent theoretical description is provided including different aspects of the problem that will play a fundamental roll in the design and optimization of the loudspeaker. An initial experimental characterization is also provided showing the viability of the process, validating some presented theoretical elements, such as in-plane stress or voltage controlled resonance frequency, and also providing initial information on orders of magnitude of residual stress, dimensions feasibility or possible actuation voltage range.

Finally, a general discussion is provided considering both theoretical and experimental results providing general guidelines to further develop and optimize the loudspeaker performance.

5.2. Future work

Future work must be set on fine-optimization of the fabrication thus providing a consistent and robust process. Namely, focusing on the amorphous silicon deposition and substrate DRIE is crucial for control of the mechanical properties of the membrane, reproducibility and high yields. Extensive experimental characterization on non-linear phenomena such as squeeze-film damping is also on the horizon, which will provide important data to model this crucial effect. The study of squeeze-film damping will certainly yield pertinent information not only for the particular application of a loudspeaker but also for many MEMS applications where perforations are present.

Feedback from acoustical measurements will also provide important information for further development and optimization and comparison of the performance of clamped vs suspended geometries.

Finally, double gate structure may also be consider which present some advantages such as a wider linear rage of actuation and lower actuation voltages required.

**Acknowledgements**

The author would like to thank his adviser Prof. Joo Pedro Conde and Dr. Virgina for their guiding thought the project. Also to João Mouro, Alexandra Gualdino and Pedro Sousa for all their help and fruitfull discussions on the this work.

**References**

[1] J. Bouchaud. Mems microphones make noise in 2012, January 2012.

[2] Y. C. Chen and Y. T. Cheng. A low-power milliwatt electromagnetic microspeaker using a PDMS membrane for hearing aids application. In *Micro Electro Mechanical Systems (MEMS), 2011 IEEE 24th International Conference on*, 2011.

[3] M. C. Cheng, W. S. Huang, and S. R. S. Huang. A silicon microspeaker for hearing instruments. *Journal of Micromechanics and Microengineering*, 14(7):859, 2004.

[4] I.-J. Cho, S. Jang, and H. J. Nam. A piezoelectrically actuated mems speaker with polyimide membrane and thin film pb(zr,ti)o3(pzt) actuator. *Integrated Ferroelectrics*, 105(105):27–36, 2009.

[5] D. R. Dixon. Mems microphones break design mould, April 2006.

[6] A. Gualdino, V. Chu, and J. Conde. Pressure effects on the dynamic properties of hydrogenated amorphous silicon disk resonators. *Journal of Micromechanics and Microengineering*, 22:085026, 2012.

[7] S.-S. Je and J. Chae. A compact, low-power, and electromagnetically actuated microspeaker for hearing aids. *Electron Device Letters, IEEE*, 29(8):856 –858, aug. 2008.

[8] S. S. Je, F. Rivas, R. E. Diaz, J. Kwon, J. Kim, B. Bakkaloglu, S. Kiaei, and J. Chae. A compact and low-cost MEMS loudspeaker for digital hearing aids. *Biomedical Circuits and Systems, IEEE Transactions on*, 3(5):348358, 2009.

[9] H. Kim, A. Astle, K. Najafi, L. Bernal, P. Washabaugh, and F. Cheng. Bi-directional electrostatic microspeaker with two large-deflection flexible membranes actuated by single/dual electrodes. In *Sensors, 2005 IEEE*, page 4 pp., 30 2005-nov. 3 2005.

[10] H. J. Kim, K. Koo, S. Q. Lee, K.-H. Park, and J. Kim. High performance piezoelectric microspeakers and thin speaker array system. *ETRI Journal*, 31(6):680–687, 2009.

[11] S. Kim, X. Zhang, R. Daugherty, E. Lee, G. Kunnen, D. Allee, E. Forsythe, and J. Chae. Microelectromechanical systems (mems) based-ultrasonic electrostatic actuators on a flexible substrate. *Electron Device Letters, IEEE*, 33(7):1072 –1074, july 2012.

[12] S. C. Ko, Y. C. Kim, and S. S. Lee. Micromachined piezoelectric membrane acoustic device. *Sensors and Actuators A*, 103:1330–134, 2003.

[13] S. S. Lee and R. M. White. Piezoelectric cantilever voltage-to-frequency converter. *Sensors and Actuators A: Physical*, 71:153–157, 1998.

[14] G. Lemarquand, R. Ravaud, I. Shahosseini, V. Lemarquand, J. Moulin, and E. Lefeuvre. Mems electrodynamic loudspeakers for mobile phones. *Applied Acoustics*, 73(4):379 – 385, 2012.

[15] P. Morse and K. Ingard. *Theoretical Acoustics*. McGraw-Hill, 1968.

[16] P. Rangsten, L. Smith, L. Rosengren, and B. Hök. Electrostatically excited diaphragm driven as a loudspeaker. *Sensors and Actuators*, A(52):211–215, 1996.

[17] J. Rehder, P. Rombach, and O. Hansen. Balanced membrane micromachined loudspeaker for hearing instrument application. *Journal of Micromechanics and Microengineering*, 11:334–338, 2001.

[18] R. C. Roberts, J. Du, A. O. Ong, D. Li, C. A. Zorman, and N. C. Tien. Electrostatically driven touch-mode poly-SiC microspeaker. In *Sensors, 2007 IEEE*, 2007.

[19] P. Scheeper, A. D. van der, W. Olthuis, and P. Bergveld. A review of silicon microphones. *Sensors and Actuators A: Physical*, 44(1):1–11, 1994.

[20] I. Shahosseini, E. Lefeuvre, J. Moulin, E. Martincic, M. Woytasik, and G. Lemarquand. Optimization and microfabrication of high performance silicon-based MEMS microspeaker. *IEEE Sensors Journal*, 13:273–284, 2013.

[21] C. Shearwood, M. A. Harradine, T. S. Birch, and J. C. Stevens. Applications of polyimide membranes to MEMS technology. *Microelectronic engineering*, 30:547–550, 1996.

[22] S. H. Yi and E. S. Kim. Micromachined piezoelectric microspeaker. *Jpn. J. Appl. Phys.*, 44:3836–3841, 2005.